Journal of Radioanalytical and Nuclear Chemistry (2018) 316:233–246
https://doi.org/10.1007/s10967-018-5770-z

Molecular modeling and preclinical evaluation of radioiodinated tenoxicam for inflammatory disease diagnosis

Tamer M. Sakr[1,2] · I. T. Ibrahim[3] · Walaa H. Abd-Alla[4]

Received: 7 December 2017 / Published online: 2 March 2018

Abstract

The aim of the presented study is to investigate a new promising radiopharmaceutical tracer able to visualize and differentiate inflammation versus infection in early stages. Radioiodinated tenoxicam (*^{125}I-tenoxicam*) was prepared and its radiochemical yield and in vitro stability were assayed. The biodistribution studies were conducted on two different mice models: sterile inflammation and bacterial infection mice models. ^{125}I-tenoxicam showed high T/NT accumulation in the inflammatory tissues revealing high selectivity to the inflammatory tissues in contrast to infection bearing mice. The docking study using CDOCKER protocol for tenoxicam and radioiodinated tenoxicam with COX enzymes was performed to confirm that radioiodinated tenoxicam still retaining COX enzymes selectivity.

✉ Tamer M. Sakr
Tamer_sakr78@yahoo.com

✉ Walaa H. Abd-Alla
Walaa.abdalla@must.edu.eg

[1] Radioactive Isotopes and Generator Department, Hot Labs Center, Atomic Energy Authority, P.O. 13759, Cairo, Egypt

[2] Pharmaceutical Chemistry Department, Faculty of Pharmacy, October University of Modern Sciences and Arts (MSA), Giza, Egypt

[3] Labelled Compound Department, Hot Labs Center, Atomic Energy Authority, P.O. 13759, Cairo, Egypt

[4] Department of Pharmaceutical Chemistry, Faculty of Pharmacy, Misr University for Science & Technology, P.O. 77, 6th of October, Egypt

Graphical Abstract

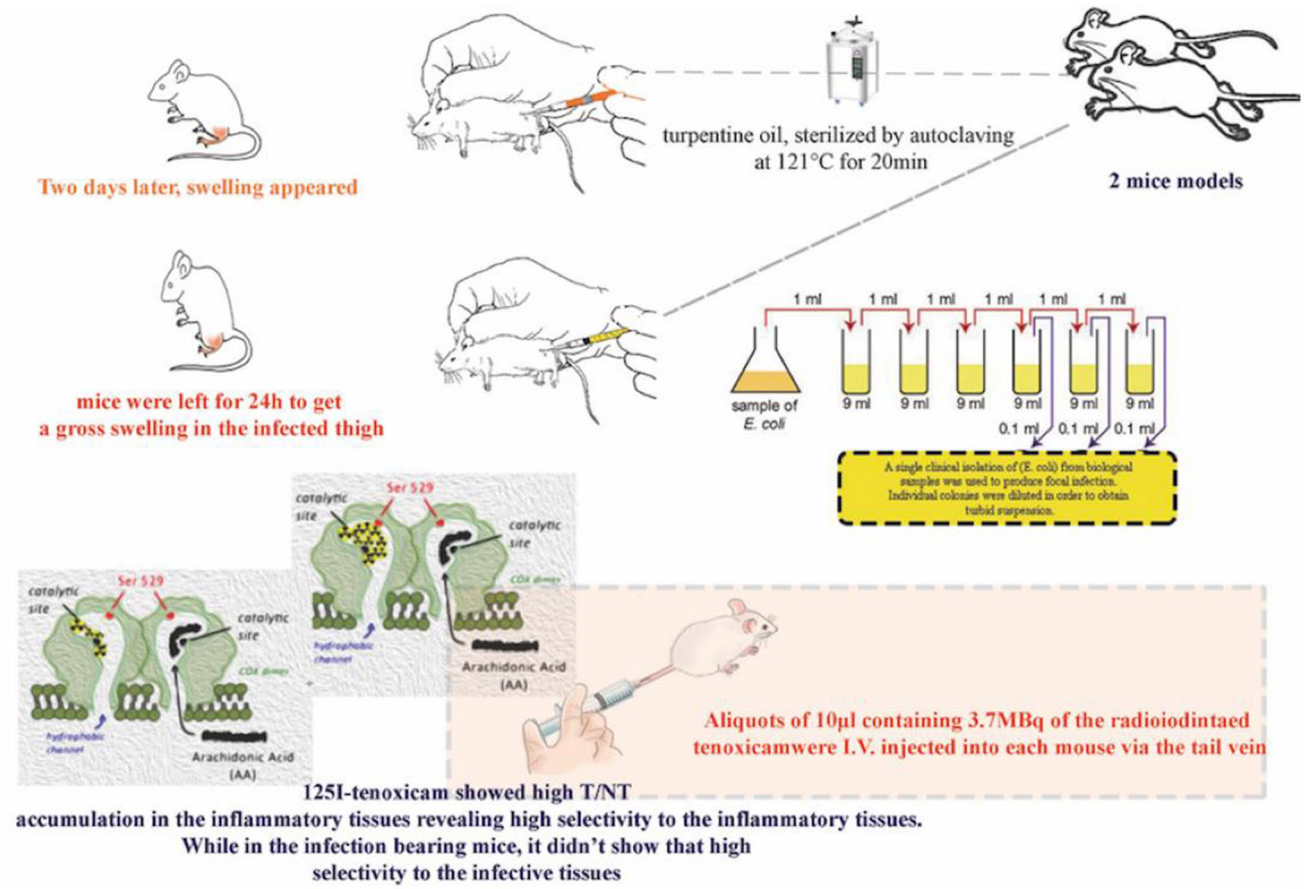

Keywords Radioiodination · Tenoxicam · Inflammation · Cyclooxygensase enzyme · Imaging · Molecular docking

Introduction

Inflammation is a normal host response that can be evoked by infection or even aseptic physical injuries. Exaggerated or sustained inflammation can lead to various human pathological consequences such as malignancy, autoimmune disorders and atherosclerosis [1]. The inflammatory response involves the production of inflammatory cytokines, prostaglandins, thromboxanes, leukotrienes and other oxidized derivatives [2]. These inflammatory mediators enhance a known sequence: vasodilation followed by high capillary permeability, accumulation of leukocytes and phagocytic cells then tissue degeneration leading to fibrosis [3]. Prostaglandins, as important inflammation mediators, are arachidonic acid derived autacoids that induce inflammatory response. Cyclooxygenase enzyme converts arachidonic acid into the prostaglandins endoperoxide precursors [4]. Cyclooxygenase has two main isoforms: COX-1 and COX-2 homodimers. COX-1 is constitutive in non-inflammatory cells, whereas COX-2 is more readily inducible in activated lymphocytes, polymorphonuclear cells and other inflammatory cells [5]. COX-1 and COX-2 molecular weight are similar, about 70 and 72 kDa, respectively. Besides, they have 65% amino acid sequence homology and nearly identical catalytic sites except for isoleucine substitution at position 523 in COX-1 with valine in COX-2 [6]. COX isoenzymes are blocked by non-steroidal anti-inflammatory drugs (NSAIDs) through competitive inhibition of their active sites by sterically hindering the entrance of the physiological binder arachidonic acid, leading to restrained generation of pro-inflammatory thromboxane, prostaglandin, and prostacyclin

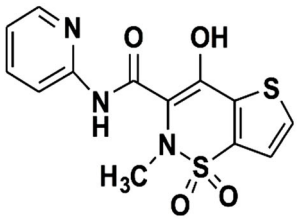

(a)

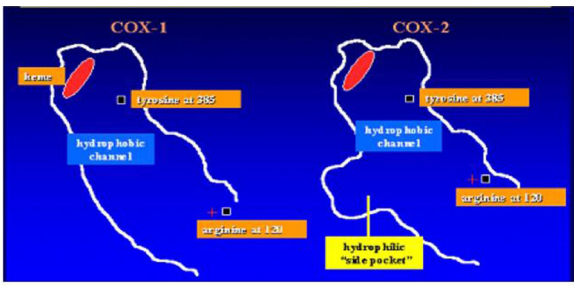

(b)

Fig. 1 **a** The chemical structure of tenoxicam, **b** active sites of COX-1 and COX-2

[4, 5]. A long hydrophobic channel representing NSAID drug binding site shows the cyclooxgenase active site. This site starts from the membrane binding domain (the lobby) to the core of the catalytic domain [7–9]. Hereby inflammation-Cox-NSAID triad is an attractive relationship to be studied in inflammation molecular imaging. Imaging techniques are emerged in the scintigraphy, including magnetic resonance imaging (MRI), positron emission tomography (PET) and single photon emission computed tomography (SPECT) to visualize and detect different biological processes inside the human body at the cellular and molecular levels [10]. Inflammatory foci can be also visualized in their early process stages when anatomical changes are not yet apparent [11]. NSAID accumulation in the inflammatory foci can be a logical leading choice of NSAID based radiotracer studying aiming for a high target/non-target ratio's. The most widely used diagnostic radiopharmaceuticals for infection imaging are ^{99m}Tc-labeled leukocytes, ^{18}F-fluorodeoxyglucose (FDG) and gallium-67 (^{67}Ga) citrate that can discriminate the infection from inflammation foci [12]. The ideal characteristics of an effective imaging radiopharmaceutical are minimal toxicity, ease of preparation, high specificity and low cost [13]. However, most of the tracers exhibited non-perfect ex vivo or in vivo findings due to inadequate binding or considerably low inflammation sensitivity such as; ^{18}F-FDG PET of inflammation may give false-positive results in cancer patients [1] and [^{11}C] rofecoxib could not detect the overexpression of COX-2 in rat models of inflammation [13]. It was reported that ^{18}F-labeled celecoxib showed high COX-2 inhibitory activity [1, 14–16]. Iodine-125 (^{125}I) is exceptionally reasonable for research examination due to its potentially high specific activity (NCA) and long radioactive decay $t_{1/2}$ (60 days) [17]. Tenoxicam (oxicam derivatives) plays an important pharmacological role as NSAID agent (Fig. 1) [16]. Based on these findings, we suggested radioiodinated tenoxicam as a promising radiotracer for inflammation imaging.

Experimental

Materials and equipment

Tenoxicam [$C_{13}H_{11}N_3O_4S_2$], chloramine-T [$ArSO_2NClNa$ (CAT)], sodium metabisulfite [$Na_2S_2O_5$], methanol [C_2H_6O], and chloroform [$CHCl_3$] were purchased from Sigma-Aldrich Company, Egypt. Whatman no 1 filter paper was purchased from Merck Company. Radioactive iodide (no-carrier added (NCA) $Na^{125}I$, 3.7 GBq/ml in 0.1 N NaOH) was granted from radioisotope production facility, Egyptian Atomic Energy Authority, Cairo, Egypt. A gamma counter (Nucleus Model 2010) connected with a well type NaI (Tl) crystal was used to measure potential of nuclear decay. Shimadzu reversed phase-HPLC that consists of pumps LC-9A, Rheodyne injector, UV spectrophotometer detector (SPD-6A) operated at a wavelength of 254 nm and a reversed-phase column (RP-18, 250 × 4.6 mm, 5 µm, Lichrosorb).

Animal model

Animal studies were done according the rules approved by the Egyptian Atomic Energy Authority (EAEA). Animal ethics committee also affirmed it. Normal Swiss albino mice (25–50 g) were brought from Helwan University, Egypt. They were sheltered in a shack in groups of five.

Radioiodination procedure

Radioiodinated tenoxicam was prepared using NCA-^{125}I in the presence of CAT that acts as an oxidizing agent. NCA-^{125}I is exceptionally reasonable for research examination due to its potentially high specific activity (NCA) and long radioactive decay $t_{1/2}$ (60 days). In an amber colored vial, discernments of tenoxicam (50-1000 µg) were dissolved in water. At that time, an aqueous solution of newly synthesized CAT (5–200 µg) was added. Then 100 µl of buffer solutions were used to adjust pH (4–12) followed by the addition of 10 µl of ^{125}I (7.2 MBq). The

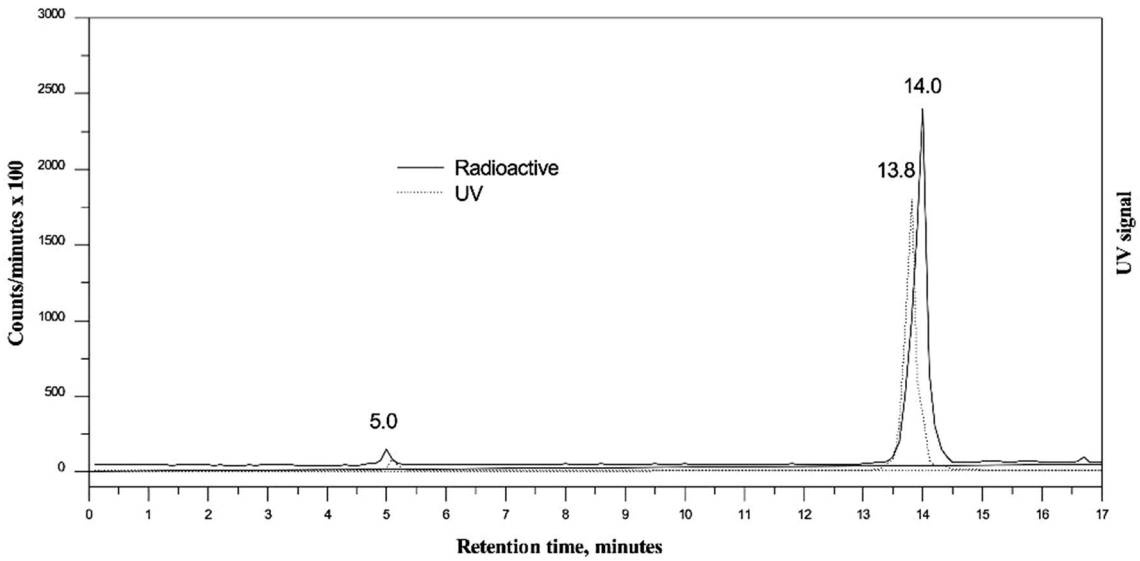

Fig. 2 HPLC radiochromatogram of radioiodinated tenoxicam

reaction mixture was swirled and kept at 25 °C. Sodium metabisulfite solution (10 mg/ml) was added at various time points to decompose extra iodine (I_2) in order to suppress the reaction. Different reaction specifications were optimized to augment the percentage of the radiochemical yield [17].

Radiochemical yield assay

Using paper chromatography and HPLC assay methods, the radiochemical yield of the radioiodinated Tenoxicam was evaluated.

Paper chromatography

Paper chromatography procedure, using Whatman no. 1 paper strips (1 cm × 13 cm), was performed. Paper chromatography strips were developed with a freshly prepared mixture of chloroform: methanol (9:1 v/v) where radioiodide ^{125}I R_f is 0–0.1 while the iodocompound (^{125}I-tenoxicam) R_f is 0.8–1. The proportion of the radioactivity of ^{125}I-tenoxicam represents the percent radiochemical yield of the ^{125}I-tenoxicam [17, 18].

Hplc

HPLC-analysis of ^{125}I-tenoxicam, as an extra affirmation, was done using Shimadzu HPLC. The HPLC was operated at 254 nm using acetonitrile: water (15:85, v/v) at rate of 1 ml/min. Then portions of 0.5 ml were separated distinctly and counted in a good-type γ-scintillation counter. An HPLC radiochromatogram is presented in Fig. 2 showing one peak at fraction No. 10 for free radioiodide (I^-), while another peak at fraction No. 28 for ^{125}I-tenoxicam that was found to match its UV signal at fraction No. 27.

In vitro stability of radioiodinated tenoxicam

The in vitro stability of radioiodinated tenoxicam was investigated at 25 °C for up to 72 h. Samples of 1–2 µl reaction mixtures were taken at various time intervals then their radiochemical yields were measured.

Biodistribution studies

Biodistribution studies of the radioiodinated tenoxicam were carried out on Swiss albino mice for two mice models, mice exhibited induced sterile inflammation and mice exhibited induced septic inflammation.

Sterile inflammation induction in mice

200 µl of sterile turpentine oil was used to induce sterile inflammation by its intramuscular administration in left thigh muscle of mice. Two days later, swelling arose [19–21].

Bacterial infection induction in mice

To attain a pathogen-induced inflammation, we carried out the following steps: *Escherichia coli* (*E. coli*) was used to acquire focal infection. Individual colonies were intramuscularly injected in 200 µl suspension in the left thigh muscle of mice. Then, the mice were kept for 24 h to get infective inflammation in thigh [19–21].

Biological assay

To determine the biological activity, bioassay was executed at intervals: 15, 60, 120 and 240 min after radioiodinated tenoxicam injection (p.i.). Proportions of 10 µl containing 3.7 MBq of the radioiodinated tenoxicam were i.v. injected to every mouse via the tail vein. Then mice were anaesthetized and weighed.

Fresh samples of separated blood, bone and muscle were taken in formerly weighed vials and assayed with ratios 7, 10 and 40% of the total body mass, respectively [22–33]. Organs were separated and placed in containers, weighed and their radioactivities were measured. Percent-injected dose per gram (% ID/g ± standard error mean (SEM)) in five mice for each time point were calculated.

Statistical analysis

Data were expressed as a mean ± SD. Statistical analysis was evaluated using Minitab 16 where one-way analysis of variance (ANOVA). Differences were considered to be significant for values of $P < 0.05$.

Molecular modeling

COX-1 and COX-2 active cavities are extending from loop of residues 111–120 representing the membrane binding region through a narrow entrance that is restricted via H-bonding network between side chains of ARG120, GLU524, TYR355 and ARG 513 (only in case of COX-2) to TYR385 at the apex of the channel. Above TYR385, the heme group is placed. Most of ligands spanned between TYR355 and TYR385. These made several specific contacts depending on their dimensions and chemical nature of functional groups. COX-1, the channel can be divided into two regions: region 1, extending from a hydrophobic pocket around TYR385 ending at GLU524 and region 2 extending from SER530 to ARG120 and a ILE portion below it. The COX-2 channel forks from the membrane end creating an extra space above His 90 and ARG513 (region 3) due to few amino acid changes [16]. The co-crystallized structure of ibuprofen with COX-1 enzyme (code: 1eqg) and celecoxib with COX-2 enzyme (code: 3ln1) were downloaded from the Brookhaven protein data bank (http://www.rcsb.org) without change in its conformation. Docking was done for our proposed structures using the compound energy as scoring function (Fig. 3) [34].

Accelrys Discovery Studio 2.5 operating system (Accelrys Inc., San Diego, CA, USA), was used to perform the molecular modeling studies. Molecules were built and their conformational models were generated automatically. The docking analysis was carried out on COX-1 and COX-2 enzymes. The 3D protein structure of COX-1 enzyme co-crystalized with ibuprofen (code: 1eqg) and COX-2 enzyme co-crystalized with celecoxib (code: 3ln1), were downloaded from the Protein Data Bank of the Research Collaboration for Structural Bioinformatics (RCSB) website [www.rcsb.org]. The cox binding pocket was docked with the lead compounds ibuprofen and celecoxib then docked with the test set compounds, after removing the water structure, protein cleaning, missing hydrogens addition and energy minimization based on DS protocol. The binding pocket of the complexed lead compounds (ibuprofen and celecoxib) with the connected amino acid molecules at sphere of radius = 7.5 Å was identified followed by docking with test compounds using CDocker module. The docking scores (-CDOCKER interaction energy) of the best-fitted conformation of each of the docked molecules as well as the total number of H-bonds with the amino acids at the binding pocket were recorded.

Results and discussion

Radioiodination of tenoxicam

Effect of chloramine-T (CAT) amount

Tenoxicam radioiodination response to CAT (5–200 µg) is illustrated in Fig. 4a. Chloramine-T (CAT), as a gentle oxidizing material, was broke down to hypochlorite anion to do the oxidation action [35, 36]. This oxidizing agent is able to modify iodine from I^- to I^+ that is capable of exhibiting an electrophilic substitution on the aromatic ring [36]. The radiochemical yield increased from 85.5 ± 1.2 to 95.1 ± 0.9% upon uprising the quantity of CAT from 5 to 25 µg. Increasing the CAT amount to be higher than 25 µg caused a decline in the radiochemical yield of ^{125}I-tenoxicam that may be due to the action of the formation of unintended oxidative side reactions [36–38].

Effect of pH

The change of pH of the reaction environment affects the radiochemical yield as shown in Fig. 4b. The ultimate radiochemical yield 95.1 ± 0.9% was obtained at pH 6 but extra pH increase in the direction alkalinity (pH 12) brings about a concomitant decline in the radiochemical yield of ^{125}I-tenoxicam down to 46 ± 1.9%. This consequence was detected previously in studies pertinent to the radio-halogenation using CAT as an oxidant. This can be interpreted

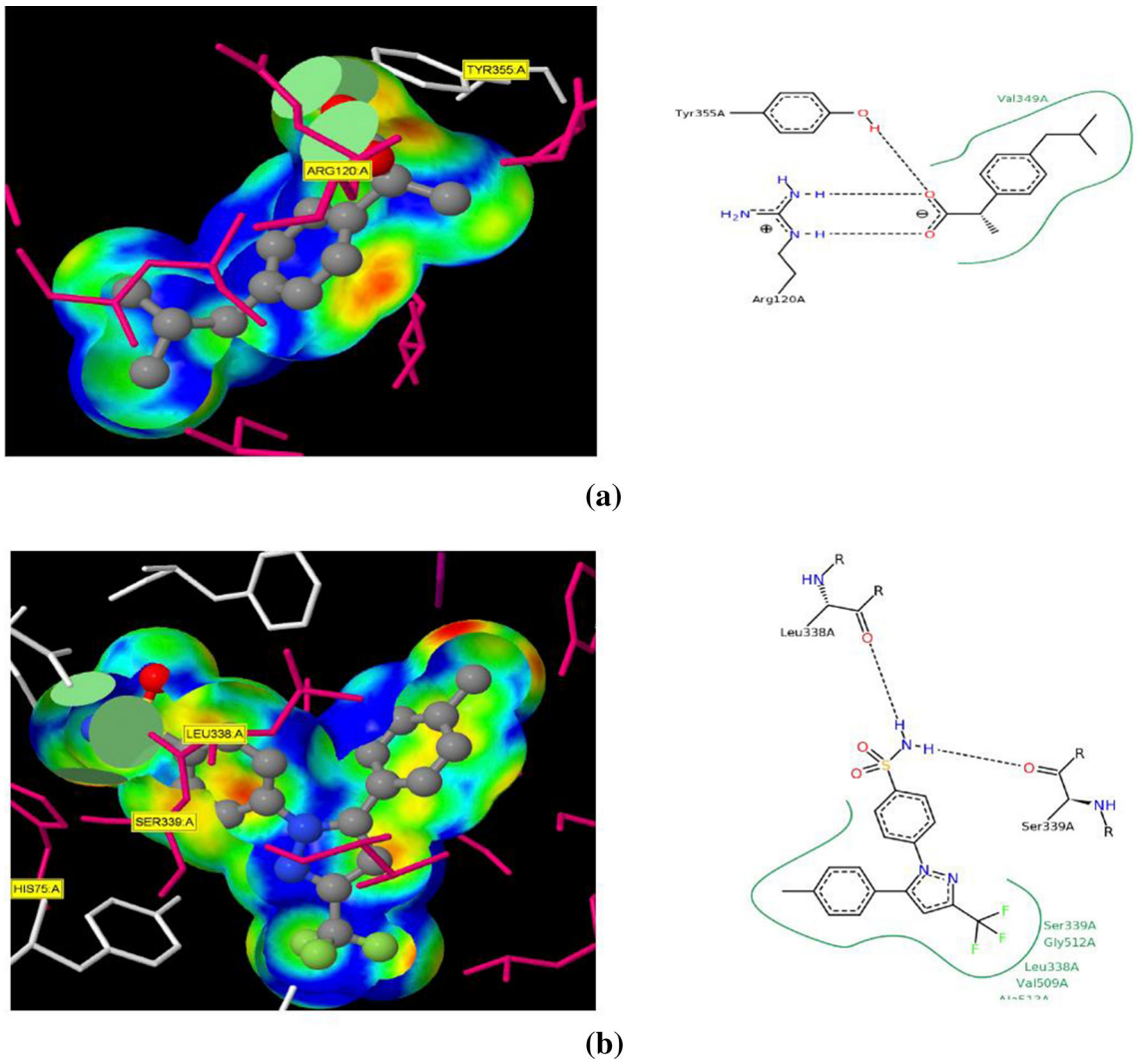

Fig. 3 The crystal structure of ibuprofen with COX-1 enzyme (**a**), the crystal structure of celecoxib with COX-2 enzyme (**b**)

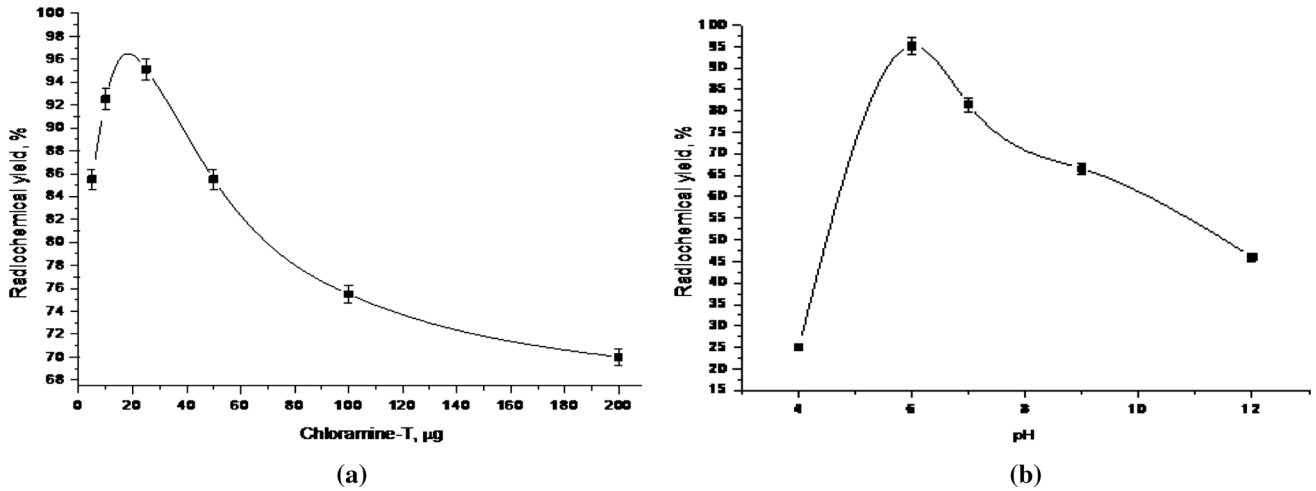

Fig. 4 Effect of chloramine-T (CAT) amount (**a**) and pH (**b**) on the radiochemical yield of radioiodinated tenoxicam

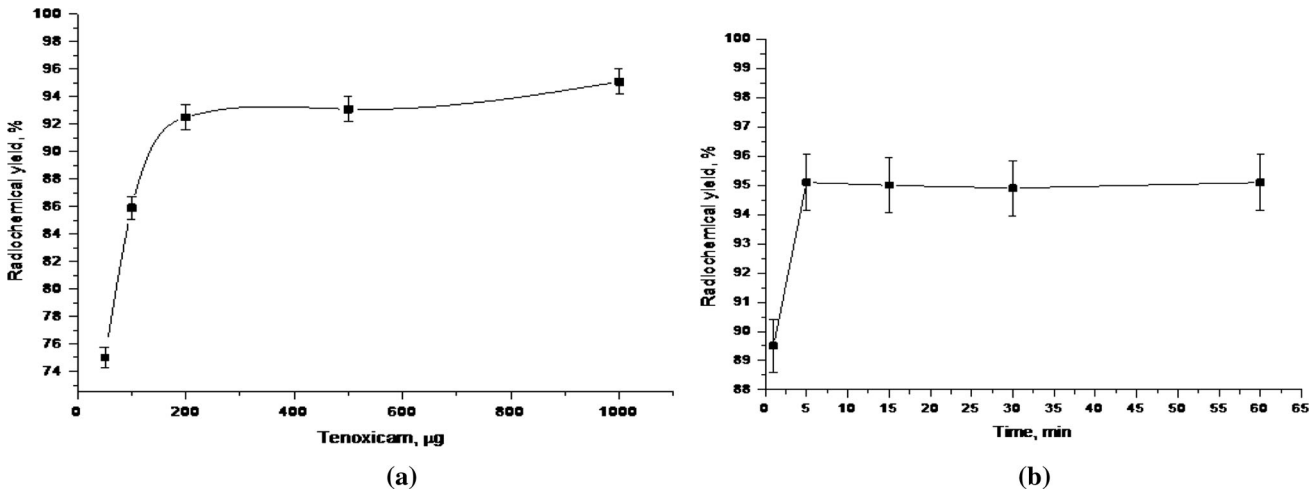

Fig. 5 Effect of tenoxicam amount (**a**) and time (**b**) on the radiochemical yield of radioiodinated tenoxicam

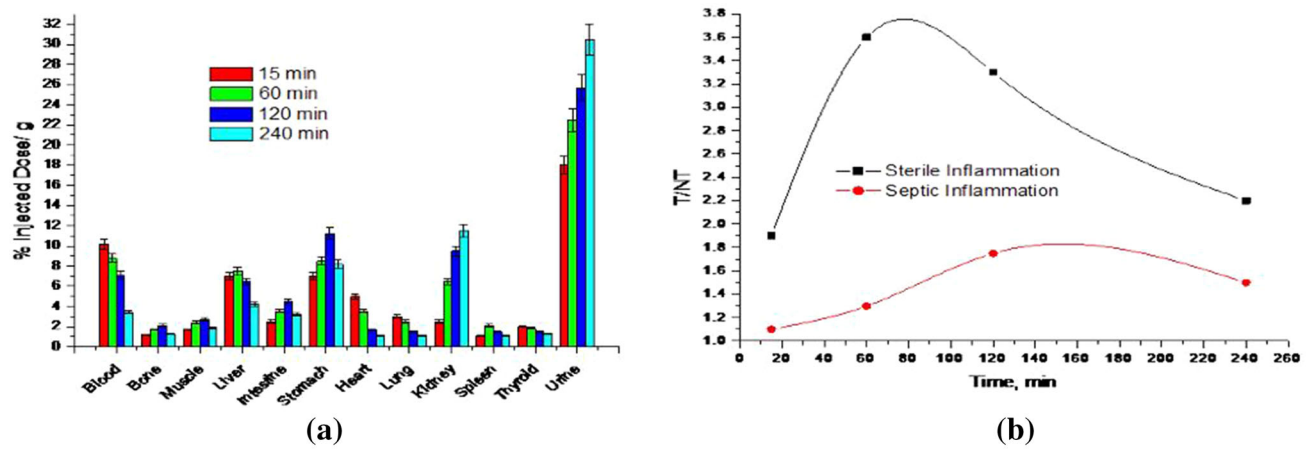

Fig. 6 In vivo biodistribution (**a**) and T/NT (**b**) of radioiodinated tenoxicam in inflammation bearing mice models at different time intervals post-injection (% ID/g ± SEM, $n = 3$). (Color figure online)

by the production of ClO^- in a high concentration of hydroxyl ions, which will pursue to oxidize iodide to hypoiodite [39–41].

Effect of tenoxicam amount

^{125}I-tenoxicam radiochemical yield is affected by tenoxicam amount as demonstrated in Fig. 5a. Escalation of tenoxicam amount from 50 to 1000 µg boosted the yield from 75 ± 1.1 to 95.1 ± 0.9%. At concentration of 1000 µg, considerable stability and superlative value of radiochemical yield was obtained, which may be attributed to the fair amount of tenoxicam to capture the entire generated iodonium ion.

Effect of reaction time

The radiochemical yield of ^{125}I-tenoxicam is vulnerable to change in reaction time that ranges from 1 to 60 min (Fig. 5b). At minute 1, the radiochemical yield was marginally low (89.5 ± 1.2%) which may be due inadequate time for the reaction between chloramine-T and iodide to produce the iodonium ion [18]. Radiochemical yield was

augmented to 95.1 ± 0.9% at reaction time above 5 min and up to 60 min.

In vitro stability of ^{125}I-tenoxicam

To determine the injection suitable time for we studied the in vitro stability of ^{125}I-tenoxicam, determination of optimum time of injection is crucial to abandon the formation of the undesired radioactive byproducts, which can accumulate in non-target organs [42–44]. ^{125}I-tenoxicam showed stability up to 24 h.

Biodistribution of ^{125}I-tenoxicam

Three mice models were used as followed: normal mice, sterile inflammation bearing mice and bacterial inflammation bearing mice, these models are used to investigate biodistribution of ^{125}I-tenoxicam. To calculate standard error, three mice were sacrificed at (15, 60, 120 and 240 min) as shown in Fig. 6a. Radioactivity levels were expressed as % injected dose per gram (% ID/g organ). The low thyroid uptake in contrast to other organs indicates that the ^{125}I-tenoxicam is free from radioiodide that is readily captured in the thyroid and confirms its in vivo stability.

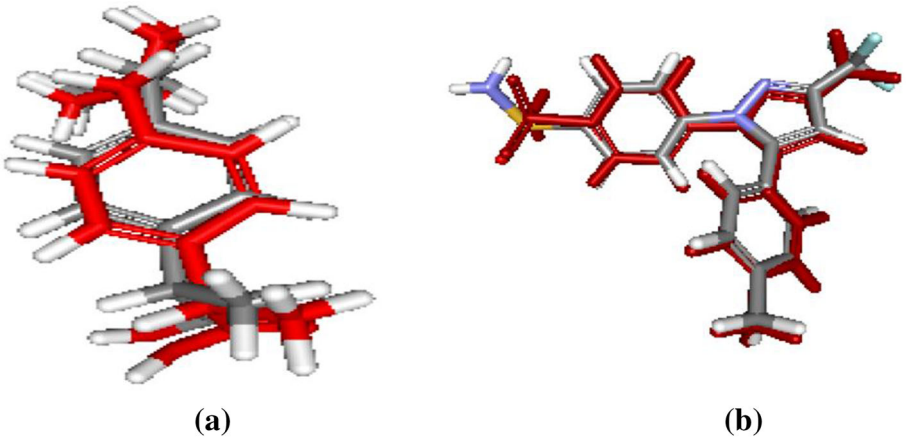

Fig. 7 **a** Alignment between the bioactive conformer of ibuprofen (colored in red) and the docked pose (colored in grey) at the COX-1 binding site and **b** alignment between the bioactive conformer of celecoxib (colored in red) and the docked pose (colored in grey) at the COX-2 binding site. (Color figure online)

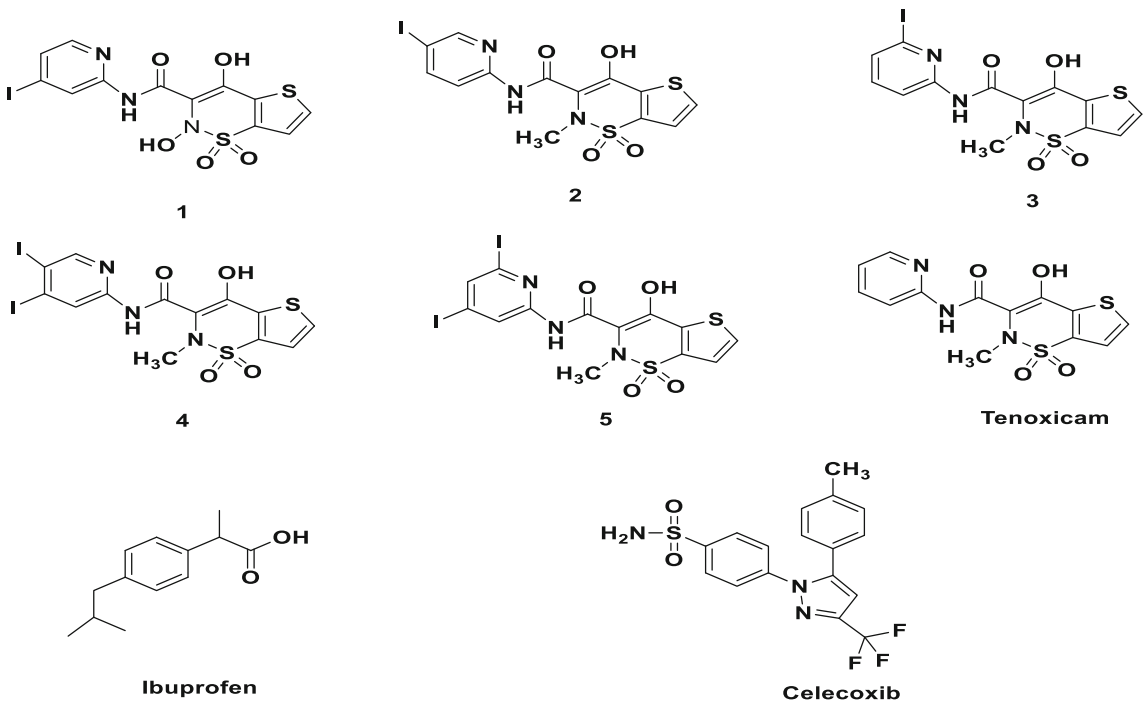

Fig. 8 2D structures of the test set compounds and lead compounds

Biodistribution in normal mice reveals that kidney is the main excretion route for ^{125}I-tenoxicam; also it didn't show any considerable accumulation in rest of body organs.

For discriminating the inflammation from infection sites, T/NT of ^{125}I-tenoxicam was evaluated. In the sterile inflammation bearing mice model, ^{125}I-tenoxicam showed high T/NT (3.6 at 1 h p.i. and 3.3 at 2 h p.i.) accumulation in the inflammatory tissues revealing high selectivity to the inflammatory tissues. In contrast to inflammation bearing mice model, the infection bearing mice didn't show that high selectivity in the infected tissues (T/NT 1.3 at 1 h p.i. and 1.75 at 2 h p.i.) (Fig 6b). So, these preclinical results prove the ability of ^{125}I-tenoxicam to act as a discriminating radiopharmaceutical imaging agent between inflamed and infected body organs due to its high selectivity to inflamed tissue that is based upon its COX enzymes targeting.

Table 1 Docking results (binding affinities, ligand amino acids interacted with the binding site on COX-1)

Compound	Docking score (kcal/mol)	Amino acids involved in H-bonds	Amino acids involved in pi-interaction
Inhibitor (Ibuprofen)	− 38.80	ARG120 (1.84 Å)	No
		TYR355 (1.92 Å)	
Tenoxicam	− 30.85	ARG120 (2.16 Å)	π-σ TYR355
		SER530 (2.01 Å)	π-+ ARG120
Compound (**1**)	− 28.36	ARG120 (2.37 Å)	π-+ ARG120
		SER530 (2.38 Å)	
		SER530 (1.87 Å)	
Compound (**2**)	− 32.94	ARG120 (2.31 Å)	No
		SER530 (2.24 Å)	
Compound (**3**)	− 28.71	ARG120 (2.21 Å)	π-+ ARG120
		SER530 (2.05 Å)	
Compound (**4**)	− 33.72	SER530 (2.19 Å)	π-π PHE381
Compound (**5**)	− 35.12	ARG120 (2.13 Å)	π-+ ARG120
		SER530 (1.98 Å)	
		ALA527 (2.34 Å)	

Table 2 Docking results (binding affinities, ligand amino acids interacted with the binding site on COX-2)

Compound	Docking score (kcal/mol)	Amino acids involved in H-bonds	Amino acids involved in pi-interaction
Inhibitor (celecoxib)	− 52.43	SER339 (1.98 Å)	π-σ SER399
		LEU338 (1.90 Å)	π-+ ARG106
Tenoxicam	− 37.83	SER516 (2.09 Å)	No
Compound (**1**)	− 37.34	TYR341 (1.91 Å)	π-σ SER399
			π-+ ARG499
Compound (**2**)	− 37.89	SER516 (2.05 Å)	No
Compound (**3**)	53.75	SER516 (2.44 Å)	π-+ ARG106
Compound (**4**)	− 41.48	SER516 (2.41 Å)	π-π PHE504
		ARG499 (2.29 Å)	
Compound (**5**)	− 29.13	SER516 (2.27 Å)	No
		ARG499 (2.14 Å)	

Ibuprofen: 2D interaction &3D interaction

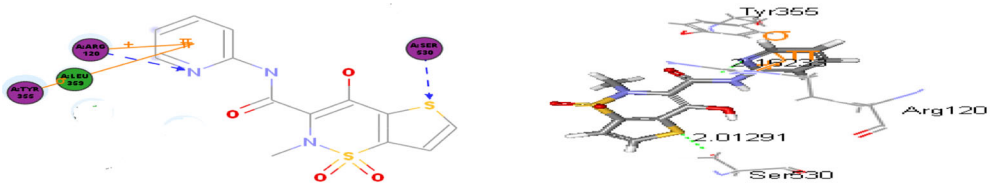

Tenoxicam: 2D interaction &3D interaction

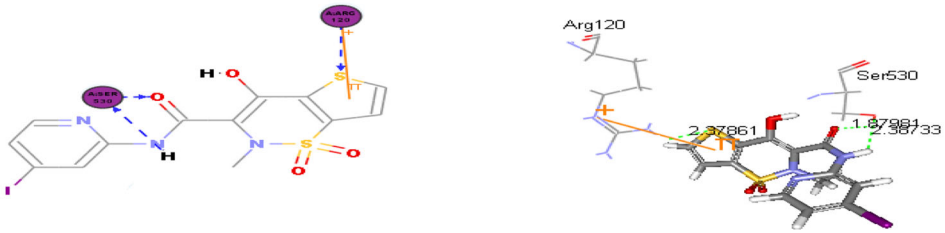

Compound (1): 2D interaction &3D interaction

Compound (2): 2D interaction &3D interaction

Compound (3): 2D interaction &3D interaction

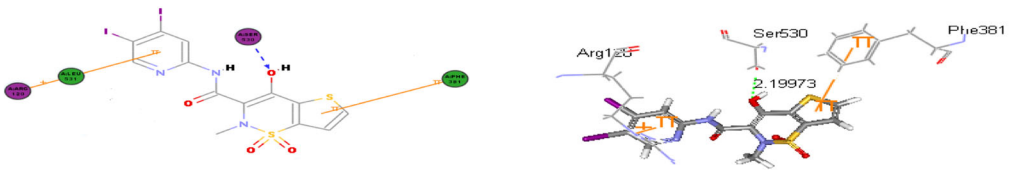

Compound (4): 2D interaction &3D interaction

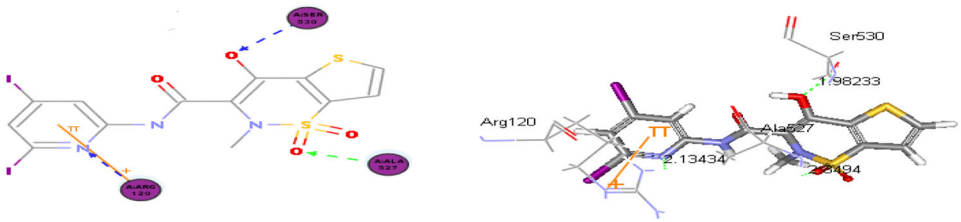

◀**Fig. 9** Binding mode of (tenoxicam + I) complexes inside the active site of COX-1 resulting from docking. The most important amino acids are shown together with their respective numbers. The hydrophobic pi interactions with the amino acids are represented as orange lines; hydrogen bonds are represented by green dashed lines (2D and 3D interaction into the active site of COX-1). (Color figure online)

Molecular modeling study

The study was done by evaluating the binding mode of bioactive conformation of the selected ibuprofen co-crystallized with COX-1 enzyme having the code: 1eqg and celecoxib co-crystallized with COX-2 enzyme (Figs. 1, 3) obtained from protein data bank without change in its conformation to study the intramolecular interactions between both of ligand and target protein. A ideal pose validation was done by alignment of the X-ray bioactive conformer with the best-fitted pose of the same compound. The alignment proved good coincidence between them (RMSD = 0.723 and 0.831 Å for ibuprofen and celecoxib, respectively), confirming the validity of the predicted pose (Fig. 7). Interactive docking using CDOCKER protocol was performed between the proposed structures and the prepared cox enzymes. Each proposed structure gave 10 possible docked poses.

We suggested different possibilities for complexation between tenoxicam and iodine then study their binding mode into cyclooxgenase binding site (Fig. 8).

The ideal pose pattern for each of the proposed molecules and the corresponding CDOCKER energy (kcal/mol) were presented to prioritize their virtual affinity to the binding site in comparison to the ideal pose of the ligand. The predicted binding energies and binding interaction of the proposed structures on COX-1 and COX-2 were illustrated in Tables 1 and 2.

In case of COX-1 enzyme, the test set compounds **1**–**5** were able to interact with cyclooxygenase binding pocket. This pocket involves such residues as AGR120, TYR385, SER530. These results show that the binding pattern of these compounds to COX-1 enzyme is similar to the co-crystal structure of ibuprofen to the binding site (Fig. 9). In case of COX-2 enzyme, the test set compounds **1**–**5** were able to interact with cyclooxygenase binding pocket. This pocket involves such residues as SER516, LEU338, ARG106, PHE504, ARG499. These results show that the binding pattern of these compounds to COX-2 enzyme is similar to the co-crystal structure of celecoxib to the binding site (Fig. 10).

Conclusion

Among the most important key promising factors in radiopharmaceutical tracers are stability and selectivity. ^{125}I-tenoxicam still gives high fitting value and good binding mode to COX-1 and COX-2 as tenoxicam that is confirmed biologically and by docking studies. Also, ^{125}I-tenoxicam showed high in vitro and in vivo stabilities. ^{125}I-tenoxicam T/NT, which is crucial for imaging success, was high in inflammation bearing mice model (3.6 at 1 h p.i.) in contrast to in infection bearing mice (T/NT 1.3 at 1 h p.i.). This introduces ^{125}I-tenoxicam as a new radiopharmaceutical agent able to differentiate between inflammation and infection foci that could be attributed to its selectivity to COX enzymes that are highly distributed in inflammation sites.

Celecoxib: 2D interaction &3D interaction

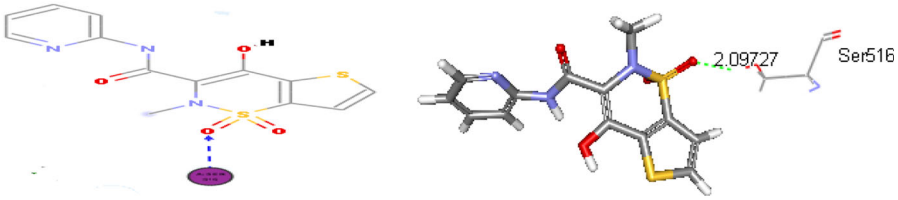

Tenoxicam: 2D interaction &3D interaction

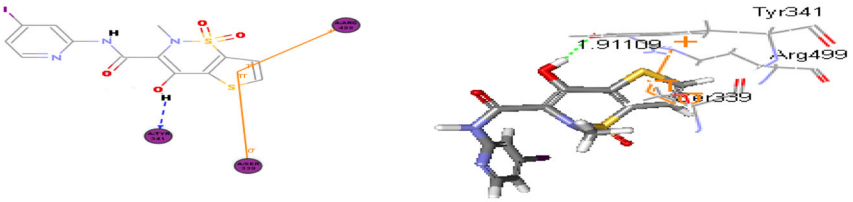

Compound (1): 2D interaction &3D interaction

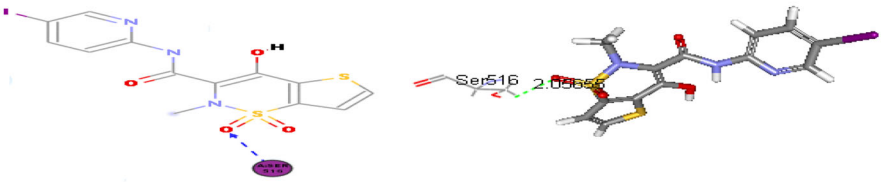

Compound (2): 2D interaction &3D interaction

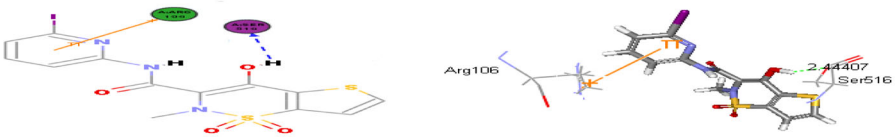

Compound (3): 2D interaction &3D interaction

Compound (4): 2D interaction &3D interaction

Compound (5): 2D interaction &3D interaction

Fig. 10 Binding mode of (tenoxicam + I) complexes inside the active site of COX-2 resulting from docking. The most important amino acids are shown together with their respective numbers. The hydrophobic pi interactions with the amino acids are represented as orange lines; hydrogen bonds are represented by green dashed lines (2D and 3D interaction into the active site of COX-2). (Color figure online)

Compliance with ethical standards

Conflict of interest Authors declare that they have no conflict of interest.

References

1. Wu C, Li F, Niu G, Chen X (2013) PET imaging of inflammation biomarkers. Theranostics 3:448–466
2. Calder PC (2006) Polyunsaturated fatty acids, inflammation, and inflammatory diseases. Am J Clin Nutr 83:S1505–1519S
3. Hilal-Dandan R, Brunton LL (2016) Pharmacotherapy of Inflammation, Fever, Pain, and Gout. In: Hilal-Dandan R, Brunton LL (eds) Goodman and Gilman's manual of pharmacology and therapeutics, 2nd edn. McGraw-Hill, New York. http://accesspharmacy.mhmedical.com/content.aspx?bookid=1810&Sectionid=124493536. Accessed 10 Jan 2017
4. Ricciotti E, FitzGerald GA (2011) Prostaglandins and inflammation. Arterioscler Thromb Vasc Biol 31:986–1000
5. Prostaglandins & Other Eicosanoids | Katzung & Trevor's Pharmacology: Examination & Board Review, 11e | AccessPharmacy | McGraw-Hill Medical
6. Kurumbail RG, Stevens AM, Gierse JK, McDonald JJ, Stegeman RA, Pak JY, Stallings WC (1996) Structural basis for selective inhibition of cyclooxygenase-2 by anti-inflammatory agents. Nature 384:644–648
7. Limongelli V, Bonomi M, Marinelli L, Gervasio FL, Cavalli A, Novellino E, Parrinello M (2010) Molecular basis of cyclooxygenase enzymes (COXs) selective inhibition. Proc Natl Acad Sci USA 107(12):5411–5416
8. Picot D, Loll PJ, Garavito RM (1994) Nature 367:243–249
9. Kurumbail RG, Kiefer JR, Marnett L (2001) Cyclooxygenase enzymes: catalysis and inhibition. J Curr Opin Struct Biol 11(6):752–760
10. Loll PJ, Picot D, Garavito RM (1995) The structural basis of aspirin activity inferred from the crystal structure of inactivated prostaglandin H2 synthase. Nat Struct Biol 2(8):637–643
11. Huub JJ, Boerman OC, Oyen WJG, Corstens FHM (2014) Imaging infection/inflammation in the new millennium. Eur J Nucl Med 28:241–252
12. Basu S, Zhuang H, Torigian DA, Rosenbaum J, Chen W, Alavi A (2009) Functional imaging of inflammatory diseases using nuclear medicine techniques. Semin Nucl Med 39:124–145
13. De Vries EFJ, Doorduin J, Dierckx RA, Van Waarde A (2008) Evaluation of [^{11}C]rofecoxib as PET tracer for cyclooxygenase 2 overexpression in rat models of inflammation. Nucl Med Biol 35(1):35–42
14. Research, C. for D. E. (n.d.). Postmarket drug safety information for patients and providers—questions and answers FDA regulatory actions for the COX-2 selective and non-selective non-steroidal anti-inflammatory drugs (NSAIDs). http://www.fda.gov/Drugs/DrugSafety/PostmarketDrugSafetyInformationforPatientsandProviders/ucm106148.htm
15. Tsopelas C (2015) Radiotracers used for the scintigraphic detection of infection and inflammation. Sci World J. https://doi.org/10.1155/2015/676719
16. Kothekar V, Sahi S, Srinivasan M, Mohan A, Mishra J (2001) Recognition of cyclooxygenase-2 (COX-2) active site by NSAIDs: a computer modelling study. Ind J Biochem Biophys 38:56–63
17. Sakr TM (2014) Synthesis and preliminary affinity testing of ^{123}I/^{125}I-N-(3-Iodo-phenyl)-2-methyl-pyrimidine-4,6-diamine, as a novel potential lung scintigraphic agent. Radiochemistry 56(2):200–206
18. Sakr TM, Motaleb MA, Zaghary WA (2015) Synthesis radioiodination and in vivo evaluation of ethyl 1,4-dihydro-7-iodo-4-oxoquinoline-3-carboxylate as a potential pulmonary perfusion scintigraphic radiopharmaceutical. J Radioanal Nucl Chem 303(1):399–406
19. Mostafa M, Motaleb MA, Sakr TM (2010) Labeling of ceftriaxone for infective inflammation imaging using ^{99m}Tc eluted from ^{99}Mo/^{99m}Tc generator based on zirconium molybdate. Appl Radiat Isot 68(10):1959–1963
20. Wei L, Bensimon C, Lockwood J, Yan X, Fernando P, Wells RG, Duan Y, Chen YX, Redshaw JR, Covitz PA (2013) Synthesis and characterization of ^{123}I-CMICE-013: a potential SPECT myocardial perfusion imaging agent. Bioorg Med Chem 21(11):2903–2911
21. Sakr TM, Motaleb MA, Ibrahim IT (2012) ^{99m}Tc-meropenem as a potential SPECT imaging probe for tumor hypoxia. J Radioanal Nucl Chem 292(2):705–710
22. Banerjee S, Pillai MRA, Ramamoorthy N (2001) Evolution of Tc-99m in diagnostic radiopharmaceuticals. Semin Nucl Med 31(4):260–277
23. Essa BM, Sakr TM, Khedr MA, El-Essawy FA, El-Mohty AA (2015) ^{99m}Tc-amitrole as a novel selective imaging probe for solid tumor: in silico and preclinical pharmacological study. Eur J Pharm Sci 76:102–109
24. Ibrahim AB, Sakr TM, Khoweysa OMA, Motaleb MA, Abd El-Bary A, El-Kolaly MT (2014) Formulation and preclinical evaluation of ^{99m}Tc-gemcitabine as a novel radiopharmaceutical for solid tumor imaging. J Radioanal Nucl Chem 302(1):179–186
25. Adachi I, Sugioka Y, Tanaka Y, Ogura Y, Nakata Y, Namba R, Tatsu Y, Nishigaki H, Sueyoshi K, Narabayashi I et al (1993) Clinical efficacy of ^{99m}Tc-tetrofosmin myocardial scintigraphy—comparison to ^{201}Tl myocardial scintigraphy. Kaku Igaku 30(4):351–362
26. Sakr TM, Essa BM, El-Essawy FA, El-Mohty AA (2014) Synthesis and biodistribution of ^{99m}Tc-PyDA as a potential marker for tumor hypoxia imaging. Radiochemistry 56(1):76–80
27. Llaurado JG (2001) The quest for the perfect myocardial perfusion indicator…still a long way to go. J Nucl Med 42(2):282–284
28. Sakr TM, El-Safoury DM, Awad GAS, Motaleb MA (2013) Biodistribution of ^{99m}Tc-sunitinib as a potential radiotracer for tumor hypoxia imaging. J Label Compd Radiopharm 56:392–395
29. Sakr TM, Moustapha ME, Motaleb MA (2013) ^{99m}Tc-nebivolol as a novel heart imaging radiopharmaceutical for myocardial infarction assessment. J Radioanal Nucl Chem 295(2):1511–1516
30. Kailasnath P, Sinusas AJ (2001) Comparison of Tl-201 with Tc-99m-labeled myocardial perfusion agents: technical, physiologic, and clinical issues. J Nucl Cardiol 8(4):482–498
31. Matsunari I, Fujino S, Taki J, Senma J, Aoyama T, Wakasugi T, Ji Hirai, Saga T, Ichiyanagi K, Hisada K (1995) Myocardial viability assessment with technetium-99m-tetrofosmin and thallium-201 reinjection in coronary artery disease. J Nucl Med 36(11):1961–1967
32. Motaleb MA, Sakr TM (2011) Synthesis and preclinical pharmacological evaluation of ^{99m}Tc-TEDP as a novel bone imaging agent. J Label Compd Radiopharm 54:597–601
33. Liu S, Li D, Shan H, Gabbaï FP, Li Z, Conti PS (2014) Evaluation of ^{18}F-labeled BODIPY dye as potential PET agents for myocardial perfusion imaging. Nucl Med Biol 41(1):120–126
34. Fernandez-Recio J, Totrov M, Abagyan R (2004) Identification of protein–protein interaction sites from docking energy landscapes. J Mol Biol 335:843–865
35. Arotsky J, Darby AC, Hamilton JB (1973) Iodination and iodo-compounds. Part IV. The effect of substituents and solvent composition on the rate of aromatic iodination by means of the tri-iodine cation. J. Chem. Soc. Perkin Trans 2:595–599

36. Adam MJ, Wilbur DS (2005) Radiohalogens for imaging and therapy. Chem Soc Rev 34(2):153–163
37. Ibrahim AB, Sakr TM, Khoweysa OMA, Motaleb MA, Abd El-Bary A, El-Kolaly MT (2015) Radioiodinated anastrozole and epirubicin as potential targeting radiopharmaceuticals for solid tumor imaging. J Radioanal Nucl Chem 303(1):967–975
38. El-Azony KM (2010) Preparation of ^{125}I-celecoxib with high purity as a possible tumor agent. J Radioanal Nucl Chem 285:315–320
39. Motaleb MA, El-Kolaly MT, Rashed HM, Abd El-Bary A (2012) Radioiodinated paroxetine, a novel potential radiopharmaceutical for lung perfusion scan. J Radioanal Nucl Chem 292:629–635
40. Cotton FA, Wilkinson G (1988) Advanced inorganic chemistry, vol 594. Wiley, New York
41. Tolmachev V, Bruskin A, Sivaev I, Lundqvist H, Sjöberg S (2002) Radiobromination of *closo*-dodecaborate anion. Aspects of labelling chemistry in aqueous solution using Chloramine-T. Radiochem Acta 90:229–235
42. Mohamed KO, Nissan YN, El-Malah AA, Ahmed WA, Ibrahim DM, Sakr TM, Motaleb MA (2017) Design, synthesis and biological evaluation of some novel sulfonamide derivatives as apoptotic agents. Eur J Med Chem 135:424–433
43. Sanad MH, Sakr TM, Abdel-Hamid WHA, Marzook EA (2017) In silico study and biological evaluation of ^{99m}Tc-tricabonyl oxiracetam as a selective imaging probe for AMPA receptors. J Radioanal Nucl Chem 314(3):1505–1515
44. Al-Wabli RI, Sakr TM, Khedr MA, Adli ASA, Motaleb MA, Zaghary WA (2016) Platelet-12 Lipoxygenase targeting via newly synthesized curcumin derivative radiolabeled with technetium-99m. Chem Cent J 10(1):73